High-pressure versus isoelectronic doping effect on the honeycomb iridate Na2 IrO3

V. Hermann, Jihaan Ebad-Allah, Florian Freund, I. M. Pietsch, Anton Jesche, Alexander A. Tsirlin, Joachim Deisenhofer, M. Hanfland, Philipp Gegenwart, Christine A. Kuntscher

Angaben zur Veröffentlichung / Publication details:

Hermann, V., Jihaan Ebad-Allah, Florian Freund, I. M. Pietsch, Anton Jesche, Alexander A. Tsirlin, Joachim Deisenhofer, M. Hanfland, Philipp Gegenwart, and Christine A. Kuntscher. 2017. "High-pressure versus isoelectronic doping effect on the honeycomb iridate Na2 IrO3." *Physical Review B* 96 (19): 195137. https://doi.org/10.1103/physrevb.96.195137.

High-pressure versus isoelectronic doping effect on the honeycomb iridate Na_2IrO_3

V. Hermann,[1] J. Ebad-Allah,[1,2] F. Freund,[3] I. M. Pietsch,[3] A. Jesche,[3] A. A. Tsirlin,[3] J. Deisenhofer,[4] M. Hanfland,[5] P. Gegenwart,[3] and C. A. Kuntscher[1,*]

[1]*Experimentalphysik II, Augsburg University, 86159 Augsburg, Germany*

[2]*Department of Physics, Tanta University, 31527 Tanta, Egypt*

[3]*Experimentalphysik VI, Center for Electronic Correlations and Magnetism, Augsburg University, 86159 Augsburg, Germany*

[4]*Experimentalphysik V, Center for Electronic Correlations and Magnetism, Augsburg University, 86135 Augsburg, Germany*

[5]*European Synchrotron Radiation Facility, Boîte Postale 220, 38043 Grenoble, France*

(Received 6 July 2017; revised manuscript received 9 October 2017; published 20 November 2017)

We study the effect of isoelectronic doping and external pressure in tuning the ground state of the honeycomb iridate Na_2IrO_3 by combining optical spectroscopy with synchrotron x-ray diffraction measurements on single crystals. The obtained optical conductivity of Na_2IrO_3 is discussed in terms of a Mott-insulating picture versus the formation of quasimolecular orbitals and in terms of Kitaev interactions. With increasing Li content x, $(Na_{1-x}Li_x)_2IrO_3$ moves deeper into the Mott-insulating regime, and there are indications that up to a doping level of 24% the compound comes closer to the Kitaev limit. The optical conductivity spectrum of single-crystalline α-Li_2IrO_3 does not follow the trends observed for the series up to $x = 0.24$. There are strong indications that α-Li_2IrO_3 is not as close to the Kitaev limit as Na_2IrO_3 and lies closer to the quasimolecular orbital picture instead. Except for the pressure-induced hardening of the phonon modes, the optical properties of Na_2IrO_3 seem to be robust against external pressure. Possible explanations of the unexpected evolution of the optical conductivity with isolectronic doping and the drastic change between $x = 0.24$ and $x = 1$ are given by comparing the pressure-induced changes of lattice parameters and the optical conductivity with the corresponding changes induced by doping.

DOI: 10.1103/PhysRevB.96.195137

I. INTRODUCTION

The 5*d* transition-metal compounds show strong spin-orbit coupling (SOC) concurrent with electronic correlations, leading to interesting electronic and magnetic properties. They are discussed in terms of various exotic ground states, like topological insulators [1–3], Mott insulators [4–8], Weyl semimetals [9–11], and spin liquids [12–15]. One important family among the 5*d* transition-metal compounds is the 213 iridates A_2IrO_3 (with A = Na, Li), which have a honeycomb layered structure consisting of IrO_6 octahedra [16–18]. Na_2IrO_3 was initially interpreted in terms of a topological insulator [1]; however, experimental and theoretical investigations showed the Mott-insulating nature [19–23] in the vicinity of a Kitaev spin liquid [14,24]. Also a band insulator picture with a quasimolecular orbital (QMO) ground state was suggested as an explanation for its insulating behavior [25,26]. Both Na_2IrO_3 and α-Li_2IrO_3 order antiferromagnetically below $T_N \approx 15$ K, excluding the realization of a "pure" Kitaev spin liquid model [27–30], while T_N systematically decreases by substituting Na atoms by Li [31].

The electronic properties of the iridates are dominated by the IrO_6 octahedra, where central Ir^{4+} ions with five 5*d* electrons are surrounded by six O^{2-} ions. In Na_2IrO_3, the octahedral crystal field (with a small trigonal distortion [32]) will largely split the Ir t_{2g} and e_g manifolds, so that all five electrons occupy the t_{2g} manifold. This t_{2g} manifold is reconstructed into lower-lying, filled $j_{\text{eff}} = 3/2$ states and half-filled $j_{\text{eff}} = 1/2$ states by the strong SOC of the heavy Ir. The Coulomb repulsion U splits the half-filled $j_{\text{eff}} = 1/2$ band into an occupied lower Hubbard band and an unoccupied upper Hubbard band, like in Sr_2IrO_4, leading to the opening of a gap [19–21] with a size of ≈340 meV, being independent of temperature [20].

The application of external pressure is a very efficient and clean way to tune the ground state of materials without introducing additional scattering centers, in contrast to chemical pressure, which works via atomic substitution. Pressure-dependent resistivity measurements on the perovskite 214 iridate Ba_2IrO_4 revealed an insulator-to-metal transition at a critical pressure of 13.4 GPa [33], while the related compound Sr_2IrO_4 showed a persistent nonmetallic behavior up to a pressure of 55 GPa [34]. In contrast, most of the pyrochlore iridates $R_2Ir_2O_7$ (with R being a rare-earth element) are already metallic at ambient conditions with an insulating or semimetallic phase at low temperatures [11,35,36]. Recently, indications for a pressure-induced quantum spin liquid state were observed for α-$RuCl_3$ [37,38], which also orders in a honeycomb lattice similar to A_2IrO_3.

Here, we study the effect of external pressure and isoelectronic doping on the electrodynamical and structural properties of the honeycomb iridate Na_2IrO_3. We further juxtapose these effects and discuss which of them is more promising for tuning the system towards the Kitaev limit.

II. METHODS

$(Na_{1-x}Li_x)_2IrO_3$ single crystals (for $x \leqslant 0.24$) were prepared by a solid-state synthesis as described previously [27,31]. Actual doping levels were determined by laser ablation inductively coupled plasma mass spectrometry (LA-ICP-MS). α-Li_2IrO_3 single crystals were grown by vapor transport of separated educts as described in Ref. [39] using elemental lithium and iridium as starting materials. The samples were

*christine.kuntscher@physik.uni-augsburg.de

characterized by x-ray diffraction, specific heat, and magnetic susceptibility measurements in order to ensure phase purity and crystal quality. No foreign phases were detected.

Room-temperature near-normal incidence reflectance spectra were measured on single crystals (*ab* plane) in the frequency range 200–38 000 cm^{-1} (0.025–4.7 eV) for Na_2IrO_3 and α-Li_2IrO_3 and in the range 200–25 000 cm^{-1} (0.025–3.1 eV) for Li-doped Na_2IrO_3. The Na_2IrO_3 and α-Li_2IrO_3 single crystals were partially transparent; thus, additional transmission measurements were performed. The reflectance and transmittance measurements were carried out with a Bruker Vertex v80 Fourier transform infrared spectrometer in combination with an infrared microscope (Bruker Hyperion) with a 15× Cassegrain objective. The intensity reflected from an Al mirror served as a reference to obtain the absolute reflectance spectra. For the transmittance spectra we measured the intensity $I_{s,trans}(\omega)$ of the radiation transmitted through the sample. As a reference the intensity $I_{ref,trans}(\omega)$ transmitted through air was used.

In the case of the pure compounds Na_2IrO_3 and α-Li_2IrO_3, a Kramers-Kronig analysis of the reflectance was combined with a direct analysis of the reflectance and transmittance ($R+T$ analysis), following Ref. [40], to obtain the real part of the optical conductivity σ_1. In the partial transparent range, σ_1 of the $R+T$ analysis is used, while in the opaque range the results from a Kramers-Kronig analysis are used [41]. Since the measured single crystals of the doped compounds $(Na_{1-x}Li_x)_2IrO_3$ were opaque in the whole measured frequency range, the optical conductivity was obtained via Kramers-Kronig analysis of the reflectance data. For the high-energy extrapolation [42] we interpolated the frequency range between the measured data and the calculated spectra above 80 000 cm^{-1} (10 eV) according to a power series in $1/\omega^s$ with s up to 4 [43]. The obtained σ_1 spectra were fitted with a simple Lorentz-oscillator model.

Pressure-dependent reflectance measurements were carried out on Na_2IrO_3 single crystals in the frequency range 200–20 000 cm^{-1} (0.025–2.5 eV). To obtain the reflectance ratio R_{sd} at the sample-diamond interface, the intensity $I_{s,refl}(\omega)$ of the radiation reflected from the sample-diamond interface was measured. As the reference, the intensity $I_{ref,refl}(\omega)$ of the radiation reflected from the inner diamond-air interface of the empty diamond-anvil cell (DAC) was used. The reflectance ratios were calculated according to $R_{sd}(\omega) = R_{dia} I_{s,refl}(\omega)/I_{ref,refl}(\omega)$, with $R_{dia} = 0.167$, which was assumed to be independent of pressure [44,45]. The reflectance ratios R_{sd} were calibrated against the simulated R_{sd} obtained from fitting the absolute reflectance outside the cell with the Lorentz model. The calibrated spectra were then fitted with a large number of Lorentz terms (variational dielectric function [46]), using the REFFIT software, to obtain the real part of the optical conductivity at various pressures.

A commercial Diacell CryoDAC-Mega (almax-easylab) DAC was used for generating pressures up to 14 GPa in the far-infrared (FIR) range, while in the midinfrared (MIR), near-infrared (NIR), and visible (VIS) ranges a custom-made Syassen-Holzapfel-type [47] DAC was used for generating pressures up to 24 GPa. Pressure was determined *in situ* by using the ruby-luminescence technique [48]. CsI powder served as quasihydrostatic pressure-transmitting medium.

Since the samples are highly air sensitive [49], they were kept inside an Ar-filled glove box. They were measured quickly after exposing them to air and were stored inside a vacuum desiccator in between measurements. The pressure-dependent spectra were observed from a freshly cleaved sample, which was quickly loaded into the DAC. The typical sample size used for pressure-dependent measurements amounted to $\approx 120\,\mu m \times 120\,\mu m$ for the FIR range and $\approx 90\,\mu m \times 90\,\mu m$ for the MIR, NIR, and VIS ranges.

The pressure dependence of the lattice parameters was determined by single-crystal x-ray diffraction (XRD) measurements using synchrotron radiation at beamline ID15B at the European Synchrotron Radiation Facility (ESRF, Grenoble, France). The wavelength of the radiation was 0.4114 Å, and more than 300 reflections were used to determine the crystal structure. Diffraction data were analyzed using the CRYSALISPRO software [50], following the established protocols for the beamline [51].

Phonon frequencies at the Γ point were obtained from density-functional theory (DFT) band-structure calculations using the internal procedure of VASP [52,53] that adopts the finite-displacement method for the calculation of phonons. The Perdew-Burke-Ernzerhof exchange-correlation potential for solids [54] was used along with a k mesh of up to 64 points in the first Brillouin zone. Given variable magnetic ground states of the honeycomb iridates considered in this work, all calculations were performed for the ferromagnetic spin configuration. We have verified that collinear antiferromagnetic order changes phonon frequencies of Na_2IrO_3 by less than 1%, and magnetic order has a negligible effect on lattice dynamics. All calculations were performed on the DFT+U+SO level because both correlations and spin-orbit (SO) coupling are integral to stabilizing the insulating state of honeycomb iridates [25,26]. The on-site Hubbard repulsion and Hund's exchange parameters of DFT+U+SO were fixed at $U_d = 2$ eV and $J_d = 0.4$ eV [14]. Their variation systematically changes phonon frequencies by a few percent without affecting any of the conclusions presented below.

III. RESULTS AND DISCUSSION

A. Isoelectronic doping

The reflectance and transmittance spectra of the measured Na_2IrO_3 crystal are depicted in Fig. 1(a). Consistent with the insulating character of the material [19,20,55–58], the overall reflectivity is low, except for the frequency range 400–600 cm^{-1} due to strong phonon excitations. The sample is opaque in almost the whole studied frequency range, as given by the transmittance spectrum [see Fig. 1(a)]. For frequencies between 600 and 2000 cm^{-1} (0.074–0.25 eV) and below 400 cm^{-1} (50 meV) we obtain a transmittance up to 5%. The corresponding optical conductivity σ_1 [Fig. 1(b)] shows a pronounced absorption feature at around 1.5 eV with an absorption onset at ∼340 meV, confirming earlier experimental reports [19,20]. Above ∼2.5 eV charge-transfer excitations between the Ir 5d and O 2p orbitals contribute to the optical conductivity spectrum.

Fitting the pronounced absorption feature with the Lorentz model revealed three main contributions: The strongest Lorentz contribution labeled C is located at 1.6 eV, and

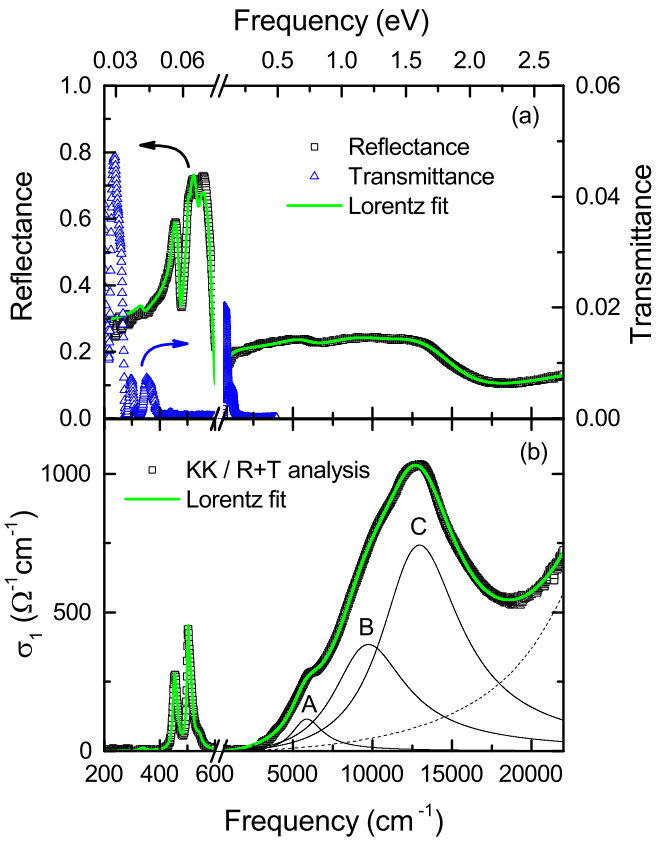

FIG. 1. (a) Reflectance (black squares) and transmittance (blue triangles) spectra of Na_2IrO_3 under ambient conditions. The green line is the fit of the reflectance spectrum with Lorentz oscillators. (b) Optical conductivity σ_1 using a combined Kramers-Kronig and $R+T$ analysis, together with the fitting with Lorentz oscillators. The pronounced absorption feature at around 1.5 eV consists of three main contributions labeled A, B, and C. The dashed line indicates the charge-transfer excitations between the Ir $5d$ and O $2p$ orbitals.

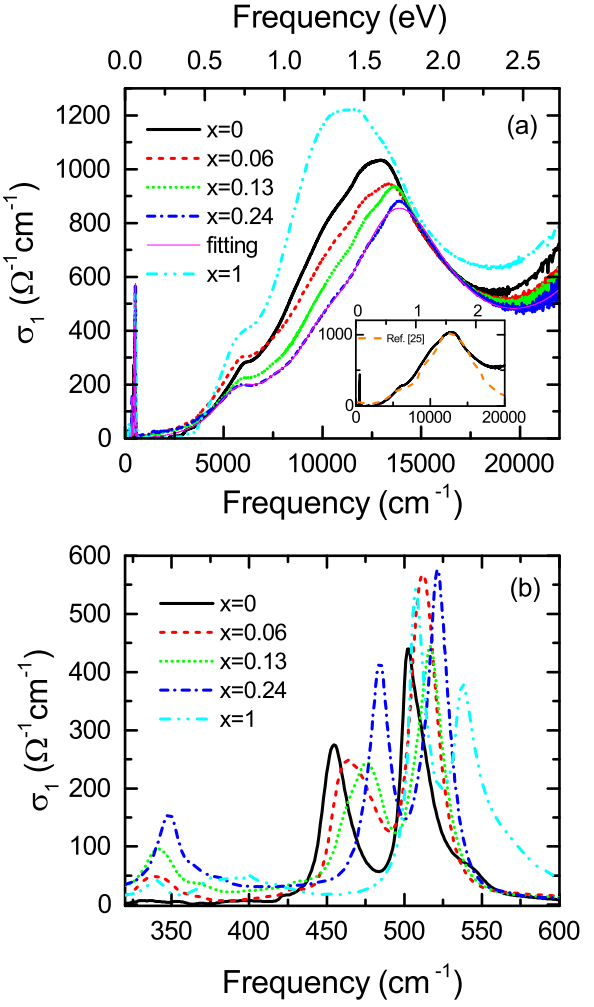

FIG. 2. Optical conductivity σ_1 of $(Na_{1-x}Li_x)_2IrO_3$ for various Li contents x (a) for the complete measured frequency range and (b) for the phonon mode range. The inset in (a) shows a comparison between calculations of Ref. [25] and our result with parameters given in the text.

two weaker contributions, A and B, are at 0.7 and 1.2 eV, respectively. These contributions can be ascribed to Ir $d-d$ transitions [19,21,25]. Compared to the findings reported by Sohn *et al.* [19], the contributions are slightly shifted in energy, and the two additional Lorentzian peaks at 0.5 and 2.0 eV are not needed to obtain a good fit of our data. Based on recent theoretical calculations, contributions A, B, and C can be ascribed to excitations between the relativistic $j_{\text{eff}} = 3/2$ ($j_{3/2}$) and $j_{\text{eff}} = 1/2$ ($j_{1/2}$) orbitals [22,24,25]. Peak C can be ascribed to intersite $j_{3/2} \rightarrow j_{1/2}$ excitations; peak B can be ascribed to weaker intersite $j_{1/2} \rightarrow j_{1/2}$ excitations, and peak A can be ascribed to on-site $j_{3/2} \rightarrow j_{1/2}$ excitations. These on-site excitations are expected to be weaker according to selection rules [24].

The optical conductivity spectrum of t_{2g}^5 systems with a honeycomb lattice structure was theoretically investigated recently [25], starting from a minimal microscopic model, which is able to capture the QMO band-insulating limit as well as the relativistic Mott-insulating regime, taking into account the Coulomb repulsion U, Hund's coupling J_{H}, and SOC λ. Furthermore, Kim *et al.* calculated the hole density $\overline{n}_{a1g}$ of the a_{1g} quasimolecular band at the Γ point as an indication for the QMO character of the material, which should be exactly 1 for the pure QMO state [25]. Comparing the shape of our optical conductivity to their calculated spectra with the Kubo formula and with $J_{\text{H}} = 1.6t$ (t is the hopping parameter between adjacent Ir atoms), we find the best match for λ at $1.6t$ and $U - 3J_{\text{H}} = 2.0t$. Setting t to a reasonable value of $t = 0.31$ eV, which is slightly higher than $t \approx 0.27$ eV from various theoretical calculations [26,56,59], we find a three-peak structure matching very well our obtained spectrum, as shown in the inset of Fig. 2(a). In comparison, setting $t \approx 0.27$ eV as implied by Ref. [25] will make the spectrum with $U - 3J_{\text{H}} = 3.2t$ fit to our main peak C reasonable well, but peak A is then underestimated too much. The hole density is estimated to be around $\overline{n}_{a1g} \approx 0.35$. Thus, our results indicate that Na_2IrO_3 is closer to a band-insulating QMO state than the prediction from Kim *et al.* but still within the Mott-insulating regime [25].

The effect of Li doping on the optical conductivity of Na_2IrO_3 in the frequency range of the Ir d-d transitions and the phonon modes is illustrated in Figs. 2(a) and 2(b), respectively.

Applying a simple Lorentz model with three contributions similar to those for Na_2IrO_3, we find that the main peak C shifts to higher energies with increasing Li content x up to $x = 0.24$ ($\sim$0.1 eV for $x = 0.24$), which is the highest doping level achieved in our samples, whereas the lowest-energy contribution A is stable regarding Li substitution, with only a slight tendency towards lower energy. The overall spectral weight of the d-d excitation band decreases with increasing doping level. One further notices a small spectral weight contribution below $\sim$340 meV for the Li-doped samples compared to pure Na_2IrO_3. According to the calculations of Kim *et al.* [25], the decrease in the spectral weight along with a shift of the main excitation C to higher energies can refer to an increase of the $(U - 3J_H)/t$ value, thereby going more into the Mott-insulating regime, which is quite surprising and will be discussed in Sec. III C.

For pure α-Li_2IrO_3 we find a charge gap very similar in size ($\sim$340 meV) to that for Na_2IrO_3, consistent with theoretical predictions [22,24]. However, the optical conductivity spectrum does not follow the above-described trends for the Ir d-d transitions, which we observe for the Li-doped Na_2IrO_3 compounds. Compared to Na_2IrO_3, the overall spectral weight of the d-d excitations is increased, with the main contribution centered at around 1.4 eV, i.e., at considerably lower energy than in Na_2IrO_3. An increase in spectral weight between 0.7 and 1.5 eV was theoretically predicted for α-Li_2IrO_3 [22,24]. In particular, in contrast to Na_2IrO_3 the direct metal-metal hopping was shown to be significant in the case of α-Li_2IrO_3, which leads to additional spectral weight of $j_{1/2} \rightarrow j_{1/2}$ excitations located at around 1.1 eV. This is in accordance with the calculations of Kim *et al.* [25] for Na_2IrO_3. The increase in the spectral weight along with a shift of the main peak to lower energies is a signal for a reduction in the $(U - 3J_H)/t$ value, simply explained by an increase in the hopping parameter t due to the decrease in lattice parameters. This brings α-Li_2IrO_3 closer to the QMO limit than Na_2IrO_3.

Furthermore, the honeycomb lattices of A_2IrO_3 are discussed in terms of Kitaev interactions [14,28,60–63]. According to Li *et al.* [24], the Kitaev limit will be most closely approached by the $(Na_{1-x}Li_x)_2IrO_3$ compound with the lowest spectral weight near $\omega \approx 1.1$ eV, where the spectral weight is contributed by intersite $j_{1/2} \rightarrow j_{1/2}$ excitations. They furthermore claim that the values of the corresponding direct metal-metal hopping integrals are directly related to the magnetic interactions and that the Kitaev limit will be obtained only when the direct metal-metal hopping is small in comparison to the oxygen-assisted intersite hopping. Following this interpretation would identify the 24% doped $(Na_{0.76}Li_{0.24})_2IrO_3$ as the closest of the measured materials to the Kitaev limit signaled by the decrease in contribution B, while the enhanced direct metal-metal hopping signals that α-Li_2IrO_3 should be less close to the Kitaev limit compared to Na_2IrO_3 [14,24]. The proposed shift toward the Kitaev limit upon Li substitution is consistent with the reduction in T_N from 15 K at $x = 0$ to 6 K at $x = 0.24$. On the other hand, at $x = 1$ the T_N of about 15 K is recovered [31].

Next we focus on the analysis of the phonon mode spectrum of Na_2IrO_3 and its changes with Li doping. Experimentally, we observe up to six phonon modes which are listed in Table I and whose frequencies are plotted in Fig. 6(c) as a function of Li doping level x. With increasing Li content x all observed phonon modes harden [see also Fig. 2(b)]. The fit of the phonon mode spectrum with Lorentz oscillators is depicted in Fig. 3(a) for the Li concentration $x = 0.13$ as an example, together with the labeling of the five phonon modes. Phonon mode 1 is observed only in samples containing Li (note that for the pure Li compound, phonon mode 1 is present but the absolute value of the optical conductivity could not be determined due to technical reasons, namely, very low intensity of the transmission for the $R + T$ analysis). An additional mode 6 is observed only in the pure compounds Na_2IrO_3 and α-Li_2IrO_3 and not in the doped compounds.

TABLE I. Experimentally observed phonon frequencies (in cm^{-1}) for Na_2IrO_3, $(Na_{0.76}Li_{0.24})_2IrO_3$, and α-Li_2IrO_3 at ambient pressure.

Mode	Na_2IrO_3	$(Na_{0.76}Li_{0.24})_2IrO_3$	α-Li_2IrO_3
1		347	387
2	452	475	506
3	460	484	512
4	502	510	537
5	511	522	540
6	542		566

DFT+U+SO calculations provide microscopic insight into Γ-point phonons probed in the optical measurements. The

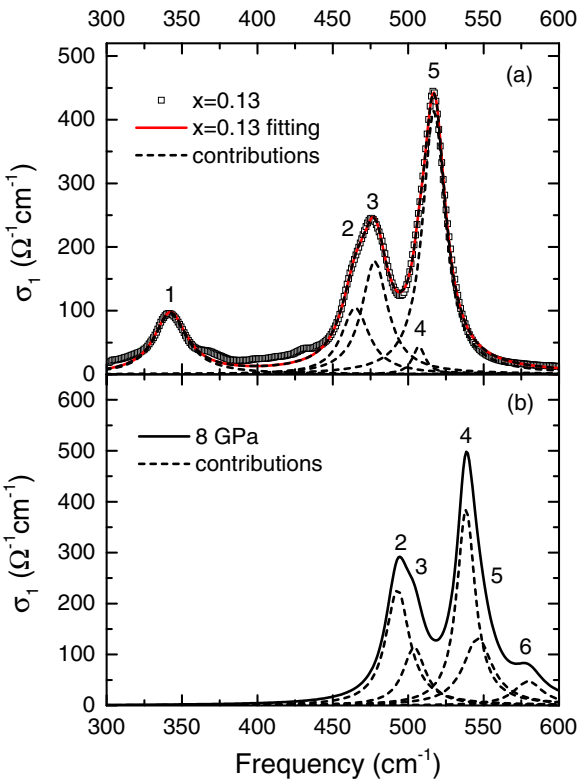

FIG. 3. Optical conductivity σ_1 of $(Na_{1-x}Li_x)_2IrO_3$ in the phonon mode range: (a) For $x = 0.13$ at ambient pressure together with the fitting with the Lorentz model and Lorentzian contributions 1 to 5. (b) For $x = 0$ at a pressure of 8 GPa together with Lorentzian contributions 2 to 6.

TABLE II. Calculated Γ-point phonon frequencies (in cm^{-1}) for Na_2IrO_3 ($x = 0$) at ambient pressure, compressed Na_2IrO_3 (comp.; with lattice parameters of the $x = 0.24$ sample but no Li substitution), $Na_{1.5}Li_{0.5}IrO_3$ ($x = 0.25$, with lattice parameters of the $x = 0.24$ sample and placing Li atoms into the center of the Ir hexagons) at ambient pressure, and α-Li_2IrO_3 ($x = 1.0$) at ambient pressure. For each mode, the atoms with largest displacements are listed.

Mode		Na_2IrO_3	Atoms	Na_2IrO_3 comp.	$x = 0.25$	Atoms	α-Li_2IrO_3
c1	A_u	544	O	567	570	O	579
c2	A_u	503	Ir-O	525	532	Ir-O-Li	528
c3	B_u	502	Ir-O	518	535	Ir-O-Li	542
c4	B_u	497	Ir-O	515	525	Ir-O-Li	527
c5	A_u	454	Ir-O	506	485	Ir-O-Li	501
c6	B_u	453	Ir-O	507	484	Ir-O-Li	503
c7	B_u	425	Na-O	469	369	Li	406
c8	A_u	413	Na-O	463	361	Li	385
c9	B_u	379	Na-O	453	346	Li	392
c10	B_u	288	Na	299	344	Li	331
c11	A_u	269	Na	289	336	Li	337
c12	B_u	267	Na	283	310	Li	314

$C2/m$ symmetry of the crystal structure allows 18 infrared-active modes that are split into 7 modes of the A_u symmetry and 11 modes of the B_u symmetry. Their frequencies and natures are listed in Table II, where we restrict ourselves to modes above 250 cm^{-1} because low-energy modes are less characteristic and were not probed in our experiment.

In Na_2IrO_3, only the high-frequency mode c1 at 544 cm^{-1} [mode 6 in Fig. 6(c) below] is a purely oxygen based vibration. Five modes, c2–c6, found between 453 and 503 cm^{-1} entail significant contributions of Ir and can be seen as collective vibrations of the Ir-O framework. Experimentally, we resolve only four modes in this frequency range [modes 2–5 in Fig. 6(c) below] because some of the modes are nearly degenerate. Three further modes, c7–c9, found between 379 and 425 cm^{-1} and not observed experimentally, presumably due to their low oscillator strengths, are Na-O vibrations, whereas further infrared-active modes positioned below 288 cm^{-1} are dominated by Na atoms.

We explored the effect of Li doping by using lattice parameters of the $x = 0.24$ sample and placing Li atoms into the center of the Ir hexagons (see phonon modes in Table II, column $x = 0.25$). The high-energy mode c1 preserves its oxygen-based nature. However, modes c2, c5, and c6, which previously did not involve Na atoms, now feature comparable contributions of Ir and Li. The spectrum at lower energies changes entirely. No equivalent of modes c7–c9 can be found, and instead, Li-based vibrations dominate the spectrum below 369 cm^{-1}. This elucidates the origin of mode 1, which was observed in the Li-doped samples but not in the pure Na_2IrO_3. Moreover, the phonon spectrum at $x = 0.25$ bears strong similarities to that of α-Li_2IrO_3 in terms of the nature of phonon modes because both Li and Ir atoms contribute to modes c2–c6. No infrared-active modes are seen in α-Li_2IrO_3 between 406 and 501 cm^{-1}, whereas below 406 cm^{-1} multiple Li-based vibrations occur.

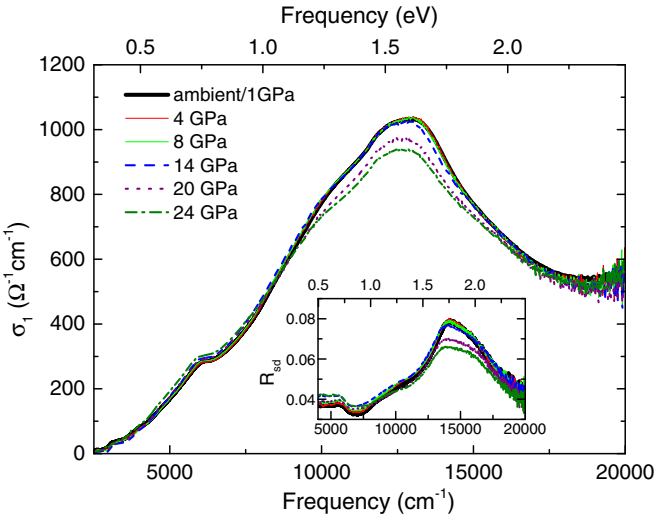

FIG. 4. Pressure-dependent optical conductivity spectra in the frequency range of the d-d excitations of Na_2IrO_3 up to 24 GPa. The inset shows the corresponding pressure-dependent reflectivity spectra R_{sd}.

Replacing atoms in a solid by isoelectronic atoms with a smaller covalent radius is expected to lead to a chemical pressure effect without any charge doping. Applying this general rule to Na_2IrO_3, one would expect a significant reduction in the lattice parameters of Na_2IrO_3 by substituting Na with smaller Li atoms. It has been shown that the changes in the lattice parameters in Na_2IrO_3 induced by Li doping are specific [31]: While the lattice parameters a and b are strongly decreased at the same rate by increasing Li content x (leading to an almost undistorted honeycomb Ir structure up to $x \leqslant 0.25$), the lattice parameter c remains almost unchanged. Hence, the c/a lattice parameter ratio increases with increasing doping x. This experimental finding was explained by the fact that Li atoms preferentially occupy the Na sites within the Ir honeycomb layers for $x \leqslant 0.25$, consistent with theoretical calculations [31]. The Na layers between the honeycomb layers remain basically unaffected for such low doping concentrations, and hence, no effective pressure is applied along the c axis. The effect of external, hydrostatic pressure on the physical properties of Na_2IrO_3 is expected to be quite different, and hence, a direct comparison with the effect of Li doping on the physical properties like crystal structure and optical response is appealing. Therefore, we studied the optical properties and crystal structure of Na_2IrO_3 single crystals as a function of external pressure.

B. External pressure

The pressure-dependent optical conductivity spectra of Na_2IrO_3 are shown in Fig. 4 in the range of the d-d excitations and in Fig. 5(b) for the phonon energy range for some selected pressures. The reflectance ratios R_{sd} are included in the corresponding figures. In the range of the d-d excitations we do not observe a significant change in the optical conductivity up to 8 GPa. For pressures above 8 GPa we observe a significant loss of spectral weight for the main excitation along with a slight shift of the three main peaks to lower energy. An

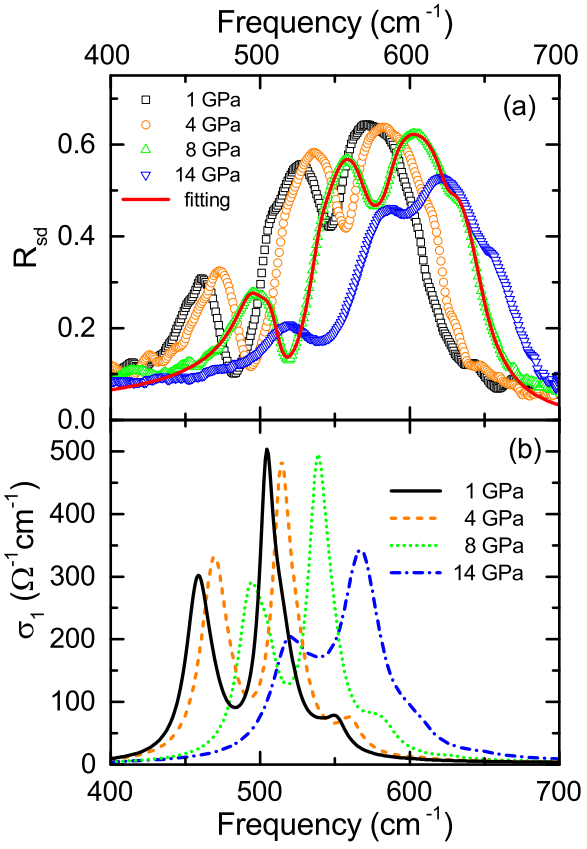

FIG. 5. (a) Pressure-dependent reflectivity spectra R_{sd} of Na_2IrO_3 in the phonon mode range for selected pressures. As an example, the fitting of the reflectivity spectrum at 8 GPa with the Lorentz model is shown. (b) The corresponding real part of the optical conductivity. With increasing pressure all phonon modes harden and show a damping above 8 GPa.

additional contribution appears at around 2.0 eV, consistent with earlier studies [19], which is more clearly observed for the higher pressures. Overall, the optical excitations in Na_2IrO_3 are quite robust regarding external pressure. These findings suggest that the $(U - 3J_H)/t$ value is not significantly affected for pressures up to 8 GPa and is only slightly decreased for higher pressures.

In Fig. 5(b) the reflectivity spectra of Na_2IrO_3 are depicted in the phonon mode range for selected pressures. In order to obtain the phonon frequencies as a function of pressure, we performed a fitting with Lorentz functions, taking into account the sample-diamond interface and the fitting of the ambient-pressure data as an extrapolation [64]. As an example, the fitting of the reflectance spectrum at 8 GPa is shown in Fig. 5(a). The so-obtained optical conductivity spectra in the phonon mode range are depicted in Fig. 5(b). We find five major phonon modes in the range 400–600 cm^{-1}, labeled 2–6 according to Fig. 3(b), consistent with the ambient-pressure data. Similar to the free-standing measurements, phonon mode 1 has an extremely small oscillator strength and is accessible only by $R + T$ analysis. Since the oscillator strength of this mode is not increased with pressure, we will not discuss it further. Like in the ambient-pressure data, we obtain two double-peak structures, with a small contribution of mode 6. There is an additional very weak contribution in the high-energy range of the phonon mode region, which is not considered in the following due to its extremely small oscillator strength.

The pressure-dependent phonon frequencies are plotted in Fig. 6(c). We observe a monotonic hardening of all five phonon modes with increasing pressure, in agreement with the DFT results (Table II). Additionally, a broadening of the modes occurs for pressures above 8 GPa (see Fig. 5). Generally, the damping of phonon modes indicates an increasing metallic character of a material which is, however, not revealed by the pressure dependence of the overall reflectivity spectrum. In other words, it is a signal for only a small decrease of the $(U - 3J_H)/t$ value, consistent with the results from the d-d excitations.

Next we discuss the effect of external pressure on the crystal structure of Na_2IrO_3 based on pressure-dependent XRD measurements carried out on single crystals. In Figs. 6(a) and 6(b) we show the evolution of the lattice parameters a, $b' := b/\sqrt{3}$, c, β, unit-cell volume V, and c/a ratio of Na_2IrO_3 as a function of external pressure in comparison to the evolution with Li doping level x, as extracted from Ref. [31]. The parameter b' allows a more direct comparison between the lattice parameters a and b regarding the pressure evolution. The pressure scale is adjusted to the doping level x for $x \leqslant 0.24$ samples using a and b', and extended to $x = 1$. The full Li substitution corresponds to an external pressure of 29 GPa.

With increasing pressure, the lattice parameters a, b', and c decrease monotonically, with the strongest effect observed for the lattice parameter c perpendicular to the Ir honeycomb layers. The effect of pressure on the lattice parameter c is approximately doubled compared to the a and b' parameters. Hence, the highest compressibility of Na_2IrO_3 is found along the c axis, which is illustrated by the c/a ratio that decreases from 1.04 to 0.99 [see Fig. 6(b)]. This effect can be ascribed to the two-dimensional nature of the Ir-O framework. The two in-plane lattice parameters a and b' are affected in a very similar manner, which excludes any pressure-induced distortion of the Ir hexagons. The angle β increases monotonically with increasing pressure [see Fig. 6(b)]. Furthermore, there is no sign of a pressure-induced structural phase transition within the measured pressure range.

In Fig. 6(a), the unit-cell volume V is plotted as a function of pressure p, as calculated from the pressure-dependent lattice parameters, together with the fit according to the Murnaghan equation of state [65],

$$V(p) = V_0[(B_0'/B_0)p + 1]^{-1/B_0'}, \quad (1)$$

with the bulk modulus $B_0 = -dp/d\ln V$ and its first derivative B_0' at ambient pressure. From the fitting we obtained $B_0 = 89.9 \pm 1.2$ GPa and $B_0' = 5.0 \pm 0.2$. In comparison, for pyrochlore iridates like $Eu_2Ir_2O_7$ and similar compounds like $Eu_2Sn_2O_7$, bulk moduli B_0 in the range 166 to 285 GPa and B_0' in the range 3.8 to 28 are reported [66–69]. For the perovskite iridate Sr_2IrO_4, $B_0 = 174 \pm 5$ GPa and $B_0' = 4.0 \pm 0.7$ are found [70], while for the stripy-honeycomb γ-Li_2IrO_3, B_0 around 130 GPa was reported recently [71]. Therefore, the bulk modulus for the honeycomb iridate Na_2IrO_3 is smaller than for pyrochlore, perovskite, and stripy-honeycomb iridates; that is, Na_2IrO_3 is more compressible. This effect can be attributed to the two-dimensional, layered character of its

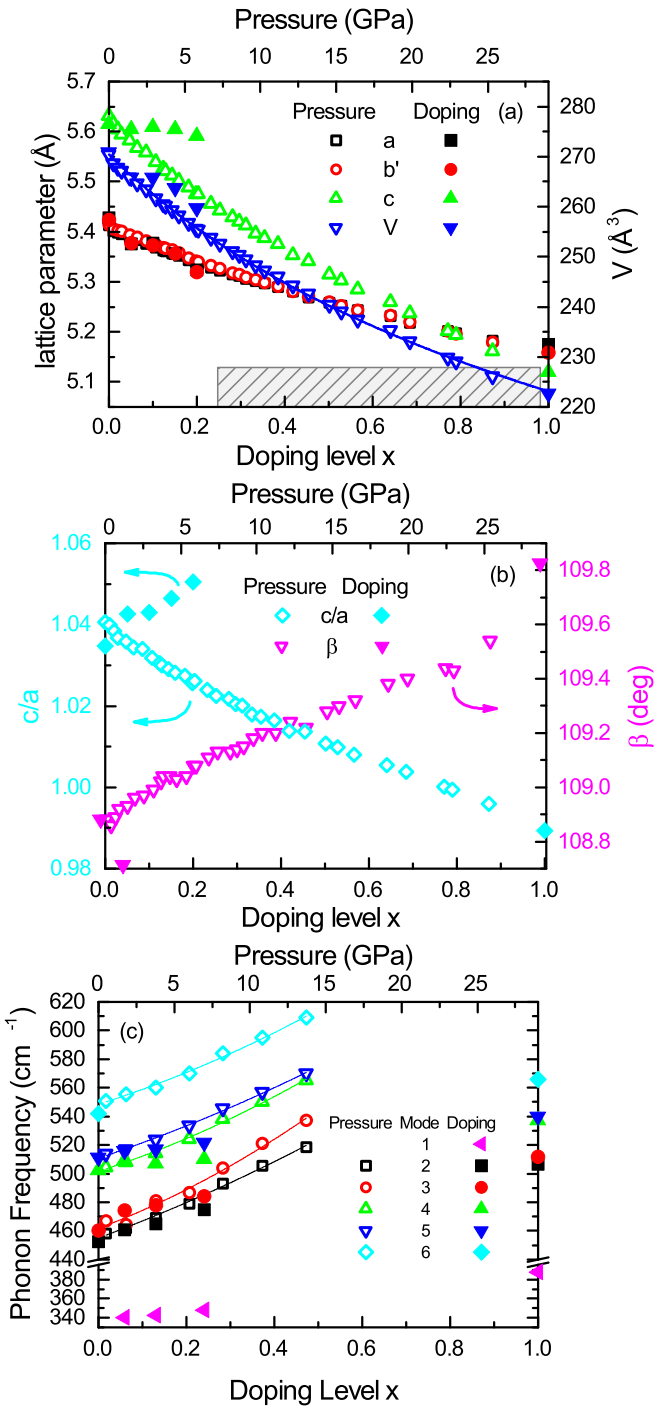

FIG. 6. (a) and (b) Lattice parameters a, $b' := b/\sqrt{3}$, c, β, unit-cell volume V, and c/a ratio of Na_2IrO_3 as a function of external pressure (open symbols) and Li doping level x (solid symbols). The results for doping levels $x = 0.05$–0.2 and $x = 1$ are extracted from Refs. [31,39], respectively. The pressure scale is adjusted to the doping level x according to the evolution of the lattice parameters a and b. The volume V is fitted by the Murnaghan equation of state as discussed in the text. The hatched area in (a) marks the miscibility gap for doping levels $0.25 < x < 1$ [31]. (c) Phonon mode frequencies as a function of external pressure and Li doping level x, keeping the pressure scaling as adjusted for the lattice parameters in (a) and (b). The solid lines are parabolic fits to the pressure-dependent mode frequencies.

crystal structure, which can be relatively easily compressed along the c axis, as illustrated by the pressure dependence of the lattice parameter c [see Figs. 6(a) and 6(b)]. This anisotropic compressibility is in line with the hierarchy of phonon modes. The Na-O bonds responsible for the compression along c are softer than their Ir-O counterparts, which determine the compressibility in the ab plane (Table II). Comparing the bulk modulus of Na_2IrO_3 with typical layered compounds like Bi_2Te_3 ($B_0 = 22$–28 GPa and $B_0' = 13.8$–17.1 for low pressures and $B_0 = 36$–38 GPa and $B_0' = 4.6$–5.5 for higher pressures) [72–74] or graphite ($B_0 = 33.8$–39 GPa and $B_0' = 8.9$–10) [75–78], however, reveals that Na_2IrO_3 is much less compressible.

C. Comparison between isoelectronic doping and external pressure

The optical conductivity identifies qualitative differences between the effects of partial Li substitution ($x \leqslant 0.24$), full Li substitution (pure α-Li_2IrO_3), and external pressure. With both increasing Li content (up to $x = 0.24$) and increasing pressure above 8 GPa, the spectral weight in the range of the d-d excitations decreases. In the case of doping, this decrease is stronger, and also a shift of the main excitation to higher energies is observed. On the contrary, full substitution with Li leads to an increase in the spectral weight along with a shift of the main excitations towards lower energies. We interpret these differences in terms of the Mott vs QMO picture and in terms of the proximity to the Kitaev limit. The partial Li substitution turns out to be most promising for approaching the Kitaev limit and, concurrently, enhances the Mott-insulating character. Full Li substitution goes in exactly the opposite direction by taking the system farther away from the Kitaev limit and toward the QMO state. The effect of external pressure is relatively mild. At pressures below 8–10 GPa, which are feasible for low-temperature magnetism studies, no visible changes in the optical conductivity occur.

These dissimilar trends are not immediately obvious from the structural perspective. Indeed, the physics of the hexagonal iridates is largely confined to the Ir-O layers, and the compression in the ab plane is about the same in all three cases [Fig. 6(a)]. Moreover, α-Li_2IrO_3 may even be viewed as Na_2IrO_3 compressed to approximately 29 GPa, when all three lattice parameters are considered. On the other hand, it seems crucial that partial Li substitution leaves the c parameter nearly unchanged, in stark contrast to the effects of external pressure and full Li substitution. Given that oxygen-assisted Ir-O-Ir hopping plays a central role in the physics of Na_2IrO_3 [24], we believe that not only the compression in the ab plane but also a change in the relative positions of Ir and O are of importance. Indeed, oxygen-mediated hoppings largely depend on the Ir-O-Ir angle, which, in turn, should be affected by the c parameter.

The difference between the fully substituted α-Li_2IrO_3 and Na_2IrO_3 compressed to 29 GPa is subtler and cannot be explained by the evolution of lattice parameters, but it becomes clearer when we consider the evolution of phonon modes. In general, one expects that compression of the structure caused by external pressure or isoelectronic doping with smaller Li atoms increases the phonon frequencies because atoms get

closer to each other and individual bonds harden. In the case of Li doping, the introduction of lighter Li atoms is a concurrent effect that should increase phonon frequencies too. Indeed, Fig. 6(c) demonstrates a steady increase in the experimental phonon frequencies, whereas the computed frequencies for c1–c6 increase as well (compare different columns in Table II). This trend no longer holds for modes c7–c9, which shift to higher frequencies upon compression of Na_2IrO_3 (see column Na_2IrO_3 comp. in Table II) but to lower frequencies upon partial or full Li substitution in pure α-Li_2IrO_3 (columns $x = 0.25$ and α-Li_2IrO_3 in Table II). It becomes even more counterintuitive when the nature of these phonon modes is considered. With heavier Na atoms replaced by lighter Li, one would hardly expect the softening of c7–c9 that occurs in α-Li_2IrO_3. This shows that, despite similar lattice dimensions, α-Li_2IrO_3 cannot be viewed as an ambient-pressure analog of Na_2IrO_3 compressed to 29 GPa.

Altogether, we see that the three effects considered in this study (partial and full Li substitution and external pressure) are all dissimilar, and among them partial Li substitution looks most promising for enhancing the Kitaev interaction term.

IV. CONCLUSION

In summary, from investigating $(Na_{1-x}Li_x)_2IrO_3$ single crystals for doping levels $x \leqslant 0.24$ and $x = 1$ by optical spectroscopy at ambient conditions we found that all measured compounds are relativistic Mott insulators despite being close to the quasimolecular orbital regime. Isoelectronic doping of Na_2IrO_3 by Li up to the doping level of $x = 0.24$ brings the material closer to the Kitaev limit and more into the Mott-insulating regime. From an experimental point of view all observed phonon modes harden with increasing Li content x due to the chemical pressure effect, while our DFT+U+SO calculations show that the nature of individual modes is changed even for low doping. Full substitution of Na by Li atoms does not follow the above trends: in α-Li_2IrO_3, the intersite $j_{1/2} \rightarrow j_{1/2}$ excitations appear to be enhanced according to the optical conductivity spectrum. Furthermore, our data suggest that α-Li_2IrO_3 is less close to the Kitaev limit and lies closer to the quasimolecular orbital regime than the Li-doped samples.

Pressure-dependent optical and x-ray diffraction measurements on Na_2IrO_3 single crystals enabled a comparison of the effect of Li doping with external pressure. With increasing pressure, the lattice parameters of Na_2IrO_3 decrease monotonically, with the largest effect found for parameter c, which is perpendicular to the honeycomb layers. The lattice parameters of α-Li_2IrO_3 are consistent with the pressure-induced changes in the lattice parameters of Na_2IrO_3 at 29 GPa, whereas for doping levels $x \leqslant 0.24$ the c lattice parameter remains unchanged. With increasing pressure all phonon modes harden, but their nature remains nearly unchanged, in contrast to the effect of Li doping. The effect of pressure on the Ir d-d excitations is much less pronounced compared to Li substitution, and we found out that partial Li substitution is most promising for tuning the system towards the Kitaev limit.

ACKNOWLEDGMENTS

We thank R. Valentí, S. Winter, and Y. Li for fruitful discussions and the European Synchrotron Radiation Facility (ESRF, Grenoble, France), for the provision of beam time. The LA-ICP-MS measurements were performed by Dr. A. Klügel, Department of Geoscience, University of Bremen. This work was financially supported by the Federal Ministry of Education and Research (BMBF), Germany, through Grant No. 05K13WA1 (Verbundprojekt 05K2013, Teilprojekt 1, PT-DESY). P.G. acknowledges financial support from the Deutsche Forschungsgemeinschaft (DFG), Germany, through TRR 80 and SPP 1666. A.J. acknowledges support from the DFG, Germany, through Grant No. JE 748/1. A.A.T. acknowledges financial support from the Federal Ministry for Education and Research via the Sofja-Kovalevskaya Award of the Alexander von Humboldt Foundation, Germany.

[1] A. Shitade, H. Katsura, J. Kunes, X.-L. Qi, S.-C. Zhang, and N. Nagaosa, Quantum Spin Hall Effect in a Transition Metal Oxide Na_2IrO_3, Phys. Rev. Lett. **102**, 256403 (2009).

[2] D. Pesin and L. Balents, Mott physics and band topology in materials with strong spin-orbit interaction, Nat. Phys. **6**, 376 (2010).

[3] B.-J. Yang and Y. B. Kim, Topological insulators and metal-insulator transition in the pyrochlore iridates, Phys. Rev. B **82**, 085111 (2010).

[4] B. J. Kim, H. Jin, S. J. Moon, J.-Y. Kim, B.-G. Park, C. S. Leem, J. Yu, T. W. Noh, C. Kim, S.-J. Oh, J.-H. Park, V. Durairaj, G. Cao, and E. Rotenberg, Novel $J_{\rm eff} = 1/2$ Mott State Induced by Relativistic Spin-Orbit Coupling in Sr_2IrO_4, Phys. Rev. Lett. **101**, 076402 (2008).

[5] B. J. Kim, H. Ohsumi, T. Komesu, S. Sakai, T. Morita, H. Takagi, and T. Arima, Phase-sensitive observation of a spin-orbital Mott state in Sr_2IrO_4, Science **323**, 1329 (2009).

[6] G. Jackeli and G. Khaliullin, Mott Insulators in the Strong Spin-Orbit Coupling Limit: From Heisenberg to a Quantum Compass and Kitaev Models, Phys. Rev. Lett. **102**, 017205 (2009).

[7] H. Watanabe, T. Shirakawa, and S. Yunoki, Microscopic Study of a Spin-Orbit-Induced Mott Insulator in Ir Oxides, Phys. Rev. Lett. **105**, 216410 (2010).

[8] C. Martins, M. Aichhorn, L. Vaugier, and S. Biermann, Reduced Effective Spin-Orbital Degeneracy and Spin-Orbital Ordering in Paramagnetic Transition-Metal Oxides: Sr_2IrO_4 versus Sr_2RhO_4, Phys. Rev. Lett. **107**, 266404 (2011).

[9] W. Witczak-Krempa and Y. B. Kim, Topological and magnetic phases of interacting electrons in the pyrochlore iridates, Phys. Rev. B **85**, 045124 (2012).

[10] A. Go, W. Witczak-Krempa, G. S. Jeon, K. Park, and Y. B. Kim, Correlation Effects on 3D Topological Phases: From Bulk to Boundary, Phys. Rev. Lett. **109**, 066401 (2012).

[11] A. B. Sushkov, J. B. Hofmann, G. S. Jenkins, J. Ishikawa, S. Nakatsuji, S. Das Sarma, and H. D. Drew, Optical evidence for a Weyl semimetal state in pyrochlore $Eu_2Ir_2O_7$, Phys. Rev. B **92**, 241108 (2015).

[12] Y. Okamoto, M. Nohara, H. Aruga-Katori, and H. Takagi, Spin-Liquid State in the $S = 1/2$ Hyperkagome Antiferromagnet $Na_4Ir_3O_8$, Phys. Rev. Lett. **99**, 137207 (2007).

[13] Y. Singh, Y. Tokiwa, J. Dong, and P. Gegenwart, Spin liquid close to a quantum critical point in $Na_4Ir_3O_8$, Phys. Rev. B **88**, 220413(R) (2013).

[14] S. M. Winter, Y. Li, H. O. Jeschke, and R. Valentí, Challenges in design of Kitaev materials: Magnetic interactions from competing energy scales, Phys. Rev. B **93**, 214431 (2016).

[15] Z. Alpichshev, F. Mahmood, G. Cao, and N. Gedik, Confinement-Deconfinement Transition as an Indication of Spin-Liquid-Type Behavior in Na_2IrO_3, Phys. Rev. Lett. **114**, 017203 (2015).

[16] S. K. Choi, R. Coldea, A. N. Kolmogorov, T. Lancaster, I. I. Mazin, S. J. Blundell, P. G. Radaelli, Y. Singh, P. Gegenwart, K. R. Choi, S.-W. Cheong, P. J. Baker, C. Stock, and J. Taylor, Spin Waves and Revised Crystal Structure of Honeycomb Iridate Na_2IrO_3, Phys. Rev. Lett. **108**, 127204 (2012).

[17] F. Ye, S. Chi, H. Cao, B. C. Chakoumakos, J. A. Fernandez-Baca, R. Custelcean, T. F. Qi, O. B. Korneta, and G. Cao, Direct evidence of a zigzag spin-chain structure in the honeycomb lattice: A neutron and x-ray diffraction investigation of single-crystal Na_2IrO_3, Phys. Rev. B **85**, 180403 (2012).

[18] S. M. Winter, A. A. Tsirlin, M. Daghofer, J. van den Brink, Y. Singh, P. Gegenwart, and R. Valenti, Models and materials for generalized Kitaev magnetism, J. Phys.: Condens. Matter. **29**, 493002 (2017).

[19] C. H. Sohn, H.-S. Kim, T. F. Qi, D. W. Jeong, H. J. Park, H. K. Yoo, H. H. Kim, J.-Y. Kim, T. D. Kang, D.-Y. Cho, G. Cao, J. Yu, S. J. Moon, and T. W. Noh, Mixing between $J_{\rm eff} = \frac{1}{2}$ and $\frac{3}{2}$ orbitals in Na_2IrO_3: A spectroscopic and density functional calculation study, Phys. Rev. B **88**, 085125 (2013).

[20] R. Comin, G. Levy, B. Ludbrook, Z.-H. Zhu, C. N. Veenstra, J. A. Rosen, Yogesh Singh, P. Gegenwart, D. Stricker, J. N. Hancock, D. van der Marel, I. S. Elfimov, and A. Damascelli, Na_2IrO_3 as a Novel Relativistic Mott Insulator with a 340-meV Gap, Phys. Rev. Lett. **109**, 266406 (2012).

[21] H. Gretarsson, J. P. Clancy, X. Liu, J. P. Hill, E. Bozin, Y. Singh, S. Manni, P. Gegenwart, J. Kim, A. H. Said, D. Casa, T. Gog, M. H. Upton, H.-S. Kim, J. Yu, Vamshi M. Katukuri, L. Hozoi, J. van den Brink, and Y.-J. Kim, Crystal-Field Splitting and Correlation Effect on the Electronic Structure of A_2IrO_3, Phys. Rev. Lett. **110**, 076402 (2013).

[22] Y. Li, K. Foyevtsova, H. O. Jeschke, and R. Valentí, Analysis of the optical conductivity for A_2IrO_3 (A = Na, Li) from first principles, Phys. Rev. B **91**, 161101 (2015).

[23] C. H. Kim, H. S. Kim, H. Jeong, H. Jin, and J. Yu, Topological Quantum Phase Transition in $5d$ Transition Metal Oxide Na_2IrO_3, Phys. Rev. Lett. **108**, 106401 (2012).

[24] Y. Li, S. M. Winter, H. O. Jeschke, and R. Valentí, Electronic excitations in γ-Li_2IrO_3, Phys. Rev. B **95**, 045129 (2017).

[25] B. H. Kim, T. Shirakawa, and S. Yunoki, From a Quasimolecular Band Insulator to a Relativistic Mott Insulator in t_{2g}^5 Systems with a Honeycomb Lattice Structure, Phys. Rev. Lett. **117**, 187201 (2016).

[26] K. Foyevtsova, H. O. Jeschke, I. I. Mazin, D. I. Khomskii, and R. Valentí, *Ab initio* analysis of the tight-binding parameters and magnetic interactions in Na_2IrO_3, Phys. Rev. B **88**, 035107 (2013).

[27] Y. Singh and P. Gegenwart, Antiferromagnetic Mott insulating state in single crystals of the honeycomb lattice material Na_2IrO_3, Phys. Rev. B **82**, 064412 (2010).

[28] Y. Singh, S. Manni, J. Reuther, T. Berlijn, R. Thomale, W. Ku, S. Trebst, and P. Gegenwart, Relevance of the Heisenberg-Kitaev Model for the Honeycomb Lattice Iridates A_2IrO_3, Phys. Rev. Lett. **108**, 127203 (2012).

[29] M. J. O'Malley, H. Verweij, and P. M. Woodward, Structure and properties of ordered Li_2IrO_3 and Li_2PtO_3, J. Solid State Chem. **181**, 1803 (2008).

[30] S. C. Williams, R. D. Johnson, F. Freund, S. Choi, A. Jesche, I. Kimchi, S. Manni, A. Bombardi, P. Manuel, P. Gegenwart, and R. Coldea, Incommensurate counterrotating magnetic order stabilized by Kitaev interactions in the layered honeycomb α-Li_2IrO_3, Phys. Rev. B **93**, 195158 (2016).

[31] S. Manni, S. Choi, I. I. Mazin, R. Coldea, M. Altmeyer, H. O. Jeschke, R. Valentí, and P. Gegenwart, Effect of isoelectronic doping on the honeycomb-lattice iridate A_2IrO_3, Phys. Rev. B **89**, 245113 (2014).

[32] B. H. Kim, G. Khaliullin, and B. I. Min, Electronic excitations in the edge-shared relativistic Mott insulator: Na_2IrO_3, Phys. Rev. B **89**, 081109 (2014).

[33] H. Okabe, N. Takeshita, M. Isobe, E. Takayama-Muromachi, T. Muranaka, and J. Akimitsu, Pressure-induced metal-insulator transition in the spin-orbit Mott insulator Ba_2IrO_4, Phys. Rev. B **84**, 115127 (2011).

[34] D. A. Zocco, J. J. Hamlin, B. D. White, B. J. Kim, J. R. Jeffries, S. T. Weir, Y. K. Vohra, J. W. Allen, and M. B. Maple, Persistent non-metallic behavior in Sr_2IrO_4 and $Sr_3Ir_2O_7$ at high pressures, J. Phys. Condens. Matter **26**, 255603 (2014).

[35] K. Ueda, J. Fujioka, Y. Takahashi, T. Suzuki, S. Ishiwata, Y. Taguchi, and Y. Tokura, Variation of Charge Dynamics in the Course of Metal-Insulator Transition for Pyrochlore-Type $Nd_2Ir_2O_7$, Phys. Rev. Lett. **109**, 136402 (2012).

[36] Y. S. Lee, S. J. Moon, S. C. Riggs, M. C. Shapiro, I. R. Fisher, B. W. Fulfer, J. Y. Chan, A. F. Kemper, and D. N. Basov, Infrared study of the electronic structure of the metallic pyrochlore iridate $Bi_2Ir_2O_7$, Phys. Rev. B **87**, 195143 (2013).

[37] Z. Wang, J. Guo, F. F. Tafti, A. Hegg, S. Sen, V. A. Sidorov, L. Wang, S. Cai, W. Yi, Y. Zhou, H. Wang, S. Zhang, K. Yang, A. Li, X. Li, Y. Li, J. Liu, Y. Shi, W. Ku, Q. Wu, R. J. Cava, and L. Sun, Observation of the quantum spin liquid state in pressurized α-$RuCl_3$, arXiv:1705.06139.

[38] Y. Cui, J. Zheng, K. Ran, J. Wen, Z. Liu, B. Liu, W. Guo, and W. Yu, A pressure-induced quantum disordered phase in α-$RuCl_3$ evidenced by NMR, arXiv:1706.02697.

[39] F. Freund, S. C. Williams, R. D. Johnson, R. Coldea, P. Gegenwart, and A. Jesche, Single crystal growth from separated educts and its application to lithium transition-metal oxides, Sci. Rep. **6**, 35362 (2016).

[40] X. Xi, C. Ma, Z. Liu, Z. Chen, W. Ku, H. Berger, C. Martin, D. B. Tanner, and G. L. Carr, Signatures of a Pressure-Induced Topological Quantum Phase Transition in BiTeI, Phys. Rev. Lett. **111**, 155701 (2013).

[41] From the $R + T$ analysis one can access the low-energy phonon modes for the partial transparent sample, which are too weak to obtain with the reflectance measurements .

[42] Reflectance and reflectance phase were calculated in the range 10 eV to 30 keV from scattering functions f_1 and f_2 of B. L. Henke, E. M. Gullikson, and J. C. Davis [X-ray interactions: Photoabsorption, scattering, transmission, and reflection at $E = 50 - 30{,}000$ eV, $Z = 1 - 92$, At. Data Nucl. Data Tables **54**, 181 (1993)] with the use of a program written by C. Porter.

[43] D. B. Tanner, Use of x-ray scattering functions in Kramers-Kronig analysis of reflectance, Phys. Rev. B **91**, 035123 (2015).

[44] M. I. Eremets and Y. A. Timofeev, Miniature diamond anvil cell: Incorporating a new design for anvil alignment, Rev. Sci. Instrum. **63**, 3123 (1992).

[45] L. Ruoff and K. Ghandehari, Refractive index of diamond anvils at high pressure, in *High Pressure Science and Technology*, edited by S. C. Schmidt, J. W. Shaner, G. A. Samara, and M. Ross, AIP Conf. Proc. Vol. 309 (AIP, New York, 1994), pp. 1523–1525.

[46] A. B. Kuzmenko, Kramers–Kronig constrained variational analysis of optical spectra, Rev. Sci. Instrum. **76**, 083108 (2005).

[47] G. Huber, K. Syassen, and W. B. Holzapfel, Pressure dependence of $4f$ levels in europium pentaphosphate up to 400 kbar, Phys. Rev. B **15**, 5123 (1977).

[48] H. K. Mao, J. Xu, and P. M. Bell, Calibration of the ruby pressure gauge to 800 kbar under quasi-hydrostatic conditions, J. Geophys. Res. **91**, 4673 (1986).

[49] J. W. Krizan, J. H. Roudebush, G. M. Fox, and R. J. Cava, The chemical instability of Na_2IrO_3 in air, Mater. Res. Bull. **52**, 162 (2014).

[50] Rigaku Oxford Diffraction, CRYSALISPRO Software system (Rigaku Corporation, Oxford, UK, 2016).

[51] M. Merlini and M. Hanfland, Single-crystal diffraction at megabar conditions by synchrotron radiation, High Pressure Res. **33**, 511 (2013).

[52] G. Kresse and J. Furthmüller, Efficiency of ab-initio total energy calculations for metals and semiconductors using a plane-wave basis set, Comput. Mater. Sci. **6**, 15 (1996).

[53] G. Kresse and J. Furthmüller, Efficient iterative schemes for *ab initio* total-energy calculations using a plane-wave basis set, Phys. Rev. B **54**, 11169 (1996).

[54] J. P. Perdew, A. Ruzsinszky, G. I. Csonka, O. A. Vydrov, G. E. Scuseria, L. A. Constantin, X. Zhou, and K. Burke, Restoring the Density-Gradient Expansion for Exchange in Solids and Surfaces, Phys. Rev. Lett. **100**, 136406 (2008).

[55] H. Jin, H. Kim, H. Jeong, C. H. Kim, and J. Yu, Mott insulating ground state and its proximity to spin-orbit insulators in Na_2IrO_3, arXiv:0907.0743.

[56] I. I. Mazin, H. O. Jeschke, K. Foyevtsova, R. Valentí, and D. I. Khomskii, Na_2IrO_3 as a Molecular Orbital Crystal, Phys. Rev. Lett. **109**, 197201 (2012).

[57] I. I. Mazin, S. Manni, K. Foyevtsova, H. O. Jeschke, P. Gegenwart, and R. Valentí, Origin of the insulating state in honeycomb iridates and rhodates, Phys. Rev. B **88**, 035115 (2013).

[58] M. Kim, B. H. Kim, and B. I. Min, Insulating nature of Na_2IrO_3: Mott-type or Slater-type, Phys. Rev. B **93**, 195135 (2016).

[59] Y. Yamaji, Y. Nomura, M. Kurita, R. Arita, and M. Imada, First-Principles Study of the Honeycomb-Lattice Iridates Na_2IrO_3 in the Presence of Strong Spin-Orbit Interaction and Electron Correlations, Phys. Rev. Lett. **113**, 107201 (2014).

[60] J. Knolle, G.-W. Chern, D. L. Kovrizhin, R. Moessner, and N. B. Perkins, Raman Scattering Signatures of Kitaev Spin Liquids in A_2IrO_3 Iridates with $A =$ Na or Li, Phys. Rev. Lett. **113**, 187201 (2014).

[61] J. Chaloupka and G. Khaliullin, Hidden symmetries of the extended Kitaev-Heisenberg model: Implications for the honeycomb-lattice iridates A_2IrO_3, Phys. Rev. B **92**, 024413 (2015).

[62] J. Chaloupka, G. Jackeli, and G. Khaliullin, Kitaev-Heisenberg Model on a Honeycomb Lattice: Possible Exotic Phases in Iridium Oxides A_2IrO_3, Phys. Rev. Lett. **105**, 027204 (2010).

[63] Y. Yamaji, T. Suzuki, T. Yamada, S.-i. Suga, N. Kawashima, and M. Imada, Clues and criteria for designing a Kitaev spin liquid revealed by thermal and spin excitations of the honeycomb iridate Na_2IrO_3, Phys. Rev. B **93**, 174425 (2016).

[64] From the Fresnel equations one obtains $R_{s-d} = |(\sqrt{\epsilon_s} - \sqrt{\epsilon_d})/(\sqrt{\epsilon_s} + \sqrt{\epsilon_d})|^2$, with ϵ_d being the dielectric function of diamond and ϵ_s being the dielectric function of the measured sample.

[65] F. D. Murnaghan, The compressibility of media under extreme pressures, Proc. Natl. Acad. Sci. USA **30**, 244 (1944).

[66] J. P. Clancy, H. Gretarsson, E. K. H. Lee, Di Tian, J. Kim, M. H. Upton, D. Casa, T. Gog, Z. Islam, B.-G. Jeon, K. H. Kim, S. Desgreniers, Y. B. Kim, S. J. Julian, and Y.-J. Kim, X-ray scattering study of pyrochlore iridates: Crystal structure, electronic, and magnetic excitations, Phys. Rev. B **94**, 024408 (2016).

[67] Y. Zhao, W. Yang, N. Li, Y. Li, R. Tang, H. Li, H. Zhu, P. Zhu, and X. Wang, Pressure-enhanced insulating state and trigonal distortion relaxation in geometrically frustrated pyrochlore $Eu_2Sn_2O_7$, J. Phys. Chem. C **120**, 9436 (2016).

[68] F. X. Zhang, M. Lang, Z. Liu, and R. C. Ewing, Pressure-Induced Disordering and Anomalous Lattice Expansion in $La_2Zr_2O_7$ Pyrochlore, Phys. Rev. Lett. **105**, 015503 (2010).

[69] S. Saha, D. V. S. Muthu, S. Singh, B. Dkhil, R. Suryanarayanan, G. Dhalenne, H. K. Poswal, S. Karmakar, S. M. Sharma, A. Revcolevschi, and A. K. Sood, Low-temperature and high-pressure Raman and x-ray studies of pyrochlore $Tb_2Ti_2O_7$: Phonon anomalies and possible phase transition, Phys. Rev. B **79**, 134112 (2009).

[70] D. Haskel, G. Fabbris, M. Zhernenkov, P. P. Kong, C. Q. Jin, G. Cao, and M. van Veenendaal, Pressure Tuning of the Spin-Orbit Coupled Ground State in Sr_2IrO_4, Phys. Rev. Lett. **109**, 027204 (2012).

[71] N. P. Breznay, A. Ruiz, A. Frano, W. Bi, R. J. Birgeneau, D. Haskel, and J. G. Analytis, Resonant x-ray scattering reveals possible disappearance of magnetic order under hydrostatic pressure in the Kitaev candidate γ-Li_2IrO_3, Phys. Rev. B **96**, 020402(R) (2017).

[72] J. O. Jenkins, J. A. Rayne, and R. W. Ure, Jr., Elastic moduli and phonon properties of Bi_2Te_3, Phys. Rev. B **5**, 3171 (1972).

[73] A. Nakayama, M. Einaga, Y. Tanabe, S. Nakano, F. Ishikawa, and Y. Yamada, Structural phase transition in Bi_2Te_3 under high pressure, High Pressure Res. **29**, 245 (2009).

[74] A. Polian, M. Gauthier, S. M. Souza, D. M. Trichês, J. Cardoso de Lima, and T. A. Grandi, Two-dimensional pressure-induced electronic topological transition in Bi_2Te_3, Phys. Rev. B **83**, 113106 (2011).

[75] O. L. Blakslee, D. G. Proctor, E. J. Seldin, G. B. Spence, and T. Weng, Elastic constants of compression-annealed pyrolytic graphite, J. Appl. Phys. **41**, 3373 (1970).

[76] M. Hanfland, H. Beister, and K. Syassen, Graphite under pressure: Equation of state and first-order Raman modes, Phys. Rev. B **39**, 12598 (1989).

[77] Y. X. Zhao and I. L. Spain, X-ray diffraction data for graphite to 20 GPa, Phys. Rev. B **40**, 993 (1989).

[78] S. Reich, C. Thomsen, and P. Ordejón, Elastic properties of carbon nanotubes under hydrostatic pressure, Phys. Rev. B **65**, 153407 (2002).